RESEARCH ARTICLE

NANO · MICRO small
www.small-journal.com

Highly Tunable Cellulosic Hydrogels with Dynamic Solar Modulation for Energy-Efficient Windows

*Noor Mohammad Mohammad, Yun Zhang, Wenhui Xu, Sai Swapneel Aranke, Daniel Carne, Pengfei Deng, Fengyin Du, Xiulin Ruan, and Tian Li**

Smart windows that can passively regulate incident solar radiation by dynamically modulating optical transmittance have attracted increasing scientific interest due to their potential economic and environmental savings. However, challenges remain in the global adoption of such systems, given the extreme variability in climatic and economic conditions across different geographical locations. Aiming these issues, a methylcellulose (MC) salt system is synthesized with high tunability for intrinsic optical transmittance (89.3%), which can be applied globally to various locations. Specifically, the MC window exhibits superior heat shielding potential below transition temperatures, becoming opaque at temperatures above the Lower Critical Solution Temperature and reducing the solar heat gain by 55%. This optical tunability is attributable to the particle size change triggered by the temperature-induced reversible coil-to-globular transition. This leads to effective refractive index and scattering modulation, making them prospective solutions for light management systems, an application ahead of intelligent fenestration systems. During the field tests, MC-based windows demonstrated a 9 °C temperature decrease compared to double-pane windows on sunny days and a 5 °C increase during winters, with simulations predicting an 11% energy savings. The ubiquitous availability of materials, low cost, and ease-of-manufacturing will provide technological equity and foster the ambition toward net-zero buildings.

1. Introduction

The growing population, rapid automation, and industrialization are expected to raise the global heating, ventilation, and air conditioning (HVAC) energy demand by 29% between 2020 and 2050, leading to a "Cold Crunch."[1,2] The building sector contributes to 40% of global energy consumption, while space conditioning systems consume 42–68% of the total building energy, depending on the environmental conditions.[3] Of this energy, a significant proportion (60%) is wasted or lost as the current building technologies are either energy inefficient or do not respond to external stimuli.[4]

Windows, serving as the main channel for heat exchange and visual discomfort, are identified as the least efficient parts of a building. Thus, energy-efficient windows that can intelligently modulate the incident solar radiation (i.e., allowing solar heat gain during winters while blocking heat gain during summers) are gaining scientific interest as they ensure human comfort, provide energy and environmental savings, and be a meaningful step toward climate change mitigation.[5] By employing dynamic fenestration systems, such as thermochromic (TC), electrochromic (EC), gasochromic, photochromic, or mechanochromic, which respond to stimuli like heat, light, voltage, or gas, buildings can achieve significant energy savings. Studies indicate that these systems can reduce HVAC and lighting energy consumption by up to 42%[6] and 85%,[7] respectively, compared to traditional buildings.

Among these strategies, the EC and TC-based windows are gaining substantial attention owing to their broad spectral range modulation, easily tunable transition temperatures, adaptability, and durability.[5] Recent studies on metal oxides[8,9] and polysaccharide-based transparent conductive oxide-glass substrates[10] suggest that EC windows demonstrated real-time applications due to their open circuit memory for extended colored state period, fast switching kinetics, high colorization efficiency, and ionic conductivity.[11] Despite these advantages, the current inorganic/polymer-based EC windows are not entirely opaque in the visible range (380–780 nm). Additionally, the manufacturing and installation costs for such convoluted systems are expensive.[11,12] This makes TC windows a more viable option as they reduce internal heating without the need for complicated architectures.[5]

Traditionally, TC window studies have focused on vanadium oxide (VO_2) and halide perovskite as thermo-chromic materials

N. M. Mohammad, Y. Zhang, W. Xu, S. S. Aranke, D. Carne, P. Deng, F. Du, X. Ruan, T. Li
School of Mechanical Engineering
Purdue University
West Lafayette, IN 47907, USA
E-mail: tianli@purdue.edu

The ORCID identification number(s) for the author(s) of this article can be found under https://doi.org/10.1002/smll.202303706

DOI: 10.1002/smll.202303706

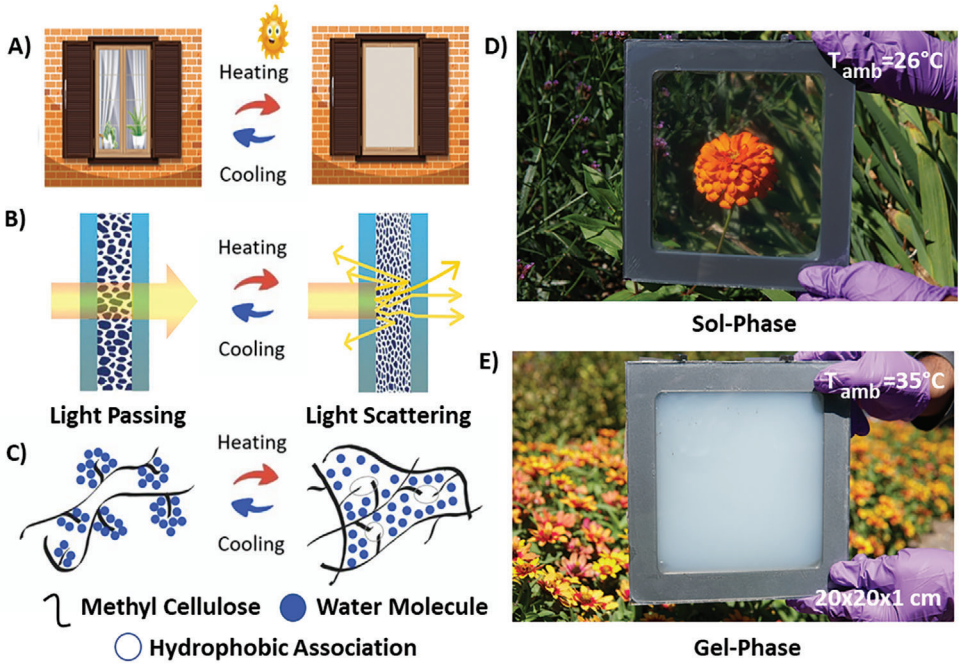

Figure 1. Phase-changing phenomena and physical demonstration. A) Schematic representation of the thermo-responsive window. B) Light scattering phenomena involved in the TR window due to changes in porosity. C) Gelation mechanism involved for phase change. D,E) Physical demonstration of the TR window activated by temperature change (D) before phase change at 26 °C and (E) after phase change at 35 °C.

with transition temperatures of 68 °C[13] and 105 °C,[14,15] respectively. These materials undergo a structural phase change from monoclinic semiconductor to tetragonal rutile metallic structure (metal–insulator transition), drastically lowering their transmittance in the infrared region and experiencing only a negligible difference in the visible range.[16] This leads to a low luminous transmittance (T_{Lum} < 60%) and solar modulation capabilities (ΔT_{solar} < 15%), limiting its large-scale commercialization.[17] Various approaches have been explored to address these limitations, including hydrothermal synthesis, chemical doping, antireflection coatings, pattern imprinting, nanoparticle dispersion, and morphological modification. These strategies aim to enhance T_{Lum} and ΔT_{solar}, with recent developments achieving values of 70.3% and 9.3%, respectively.[16,18,19] More recent advances are focused on TC materials, such as metal oxides, perovskite, liquid crystals, and hydrogels for their potential in thermal and light management systems. Notably, poly-*N*-isopropyl acrylamide (PNIPAm) and its derivatives were extensively researched, achieving optimal T_{Lum} and solar transmittance (T_{solar}) of 91.5% and 85.8% for PNIPAm-co-OA.[20–23] However, the universal acceptance of these materials has been hindered by their limited critical temperature (CT) range of ≈32 °C and the associated high fabrication costs. Moreover, these systems exhibit significant volume shrinkage due to excessive water loss during the coil-to-globule transitions, posing stability issues.[24]

Current research on TC smart windows is focused on VO_2 material stackings and organic-metallic complexes of $[(C_2H_5)_2NH_2]_2$ that can simultaneously modulate the Near-Infrared (NIR) and visible regions while providing radiative cooling (VO_2 stackings).[25–27] These systems have achieved remarkable properties, $([(C_2H_5)_2NH_2]_2$-$NiCl_4$: CT ≈46.3 °C, T_{Lum} ≈66.6% and IR modulation (ΔT_{IR}) ≈>90%; VO_2 stackings: CT ≈60 °C, T_{Lum} ≈27.8%, and ΔT_{solar} ≈9.3%), holding a great promise for large scale manufacturing. Despite these achievements, optimizing their performance remains challenging due to inherent tradeoffs between desired characteristics, and complex configurations or designs are needed to optimize their performance. Concurrently, other studies explored cellulosic polymer-based TC windows, such as hydroxypropyl cellulose and its composites, achieving CT, T_{Lum}, and ΔT_{solar} of 40 °C, 87.2%, and 80.2, respectively.[28] Yet, these studies have not explored the wide range of Lower Critical Solution Temperature (LCST) tunability or the temperature-dependent refractive index change for cellulose-based hydrogels, which are crucial for applications beyond smart windows.

To address the above-reported shortcomings, we report a simple yet effective cellulose-based TR (Thermos Responsive) window with a phase change function, adjustable based on the salt concentration, at any desired temperature between 34 °C and 72 °C with high cyclability, heat shielding, and cost-effective retrofitting capabilities. As the manufacturing is based on cellulose, the most abundant polymer in the natural world, with the advantages of non-toxicity, biocompatibility, and renewability, our window could foster advancements toward cleaner, greener, and more sustainable buildings.[29] The optical switching of TR windows is achieved by the solution-to-gel transition induced by the temperature change (**Figure 1A**). Below the transition point, the TR window material exhibits hydrophilic behavior due to the formation of O—H bonds between hydroxyl and water molecules, resulting in glass-like properties, i.e., high transparency in the visible range (Figure 1B). As the temperature reaches above the LCST, a phase-changing mechanism is triggered, leading to intermolecular hydrophobic interactions in the hydroxyl groups

(coil-to-globule transition). These interactions create hydrodynamic colloidal aggregates that tune the refractive index and solar scattering, effectively blocking sunlight (Figure 1C). This behavior is studied for the first time for the MC hydrogels using Mie theory and Monte Carlo simulations, achieving effective refractive index modulation from 1.37 at 20 °C to 1.57 at 70 °C. Unlike traditional TC materials that have fixed transition points, our MC-based TR window has a wide range of LCST tunability with excellent optical and thermal properties, such as high transmittance at room temperature ($T_{Lum} \approx 82\%$), solar modulation ($\Delta T_{solar} \approx 55\%$), and heat shielding capabilities. These properties of tunable refractive index, scattering, and high LCST tunability make these windows viable for various applications, such as beam steering, greenhouse buildings, tunable plasmonic hydrogel-based meta systems, and thermal energy storage systems.[30–32] A 20 cm × 20 cm smart window (Figure 1D,E) was fabricated to be speak its potential for reliable large-scale high-performance building applications and light management devices.

2. Results and Discussion

2.1. Transition Temperature Modulation and Structural Morphology

For global market adoption and applicability of MC hydrogel-based windows in different climatic conditions, it is crucial for these windows to exhibit tunable transition temperatures and low viscosity. These properties can be controlled for MC hydrogels through various methodologies, such as varying concentrations,[33] the addition of slats,[34] and the smart blending of other polymers.[21] To study the effects of MC and salt concentrations on the LCST, the MC concentration was adjusted from 5 to 55 g L^{-1}, while salt concentrations varied depending on their complete solubility. The MC-based thermos-responsive material preparation is elucidated in Note S1 and Figure S1 (Supporting Information). Results suggest that the transition temperature is inversely proportional to the MC concentration (72 °C at 5 g L^{-1} to 51 °C at 55 g L^{-1}) (**Figure 2A**). This is because fewer methyl groups are available at low MC concentrations. Consequently, higher activation energy is required to initiate the intermolecular hydrophobic association, leading to higher LCST (Figure S2, Supporting Information).[33] Thermodynamically, the increase in LCST is driven by the higher entropy of water molecules upon their interaction, compensating for the decrease in entropy of the hydrophobic regions.[35] Therefore, MC solutions with 25 g L^{-1} were selected for further studies for practical applications in windows due to their appropriate viscosity and transition temperature compatibility.

On the other hand, salts, especially anions, can affect the hydrophobicity of the solute, causing salting-in (chaotropic) or salting-out (kosmotropic) behavior that will control the LCST (Note S2, Supporting Information).[34] Sodium salts of 8 anions were chosen to examine the influence of anions on the transition temperature of MC. It was observed that the dissolution of salt in the MC solution (25 g L^{-1}) is a function of the ionic charges. Single-charged ions showed a concentration limit of ≈1 M, while the double-charged SO_4^{2-}, triple-charged SO_4^{3-}, and $Na_2S_2O_3^-$ based samples have concentration limits of 0.1 M, 0.05 M, and 0.6 M, respectively. Higher concentration would either increase the hydrogel's viscosity or the solute precipitation, compromising its transparency (Figure S3, Supporting Information). Except for NaI, all samples displayed positive relationships between transition temperature and concentration, signifying that salting-out behavior helps in effective LCST tuning (Figure 2B). These salts (kosmotropic), when added to the MC solution, compete with dispersed MC to attract more water molecules to surround them, resulting in higher hydrophobic micelles at any temperature.[34] This attraction of water molecules depends on the ionic charge, hydration enthalpies, and ionic radii (Figure S4, Supporting Information).[36] Therefore, mixtures of strong salts (low concentration) and weak salts (high concentration) were investigated to find an optimal thermo-responsive material with low viscosity and LCST (Table S1, Supporting Information). Our observations suggest that MC solution (25 g L^{-1}) with 0.5 M NaCl and 0.025 M Na_2PO_4 (MCSH-I) is the desired combination for our intended application with an LCST of ≈38 °C. This is because the hydrogels with LCST < 30 °C can turn opaque during winters due to an easy collapse of hydrogel structure, as window surface temperatures could reach above the transition points, leading to scattering and reflection of incident solar radiation.

To determine the gelation point (sol–gel transition temperature) of MCH-I (MC 25 g L^{-1}) and MCSH-I samples, rheological studies with dynamic temperature sweep (20 °C to 70 °C) were conducted (Note S3, Supporting Information). The crossover points of the Loss modulus (G′) and storage modulus (G″) represent the gelation point (G′ = G″) (Figure 2C). Below the gelation point, the dynamic moduli for both the samples gradually increase, and the G″ is higher than the G′, indicating a viscous fluid-like behavior (sol-phase). After the crossover, where G′ > G″, the moduli of the MCH-I steeply increase with temperature until a plateau is reached, suggesting a 3D entangled elastic polymer structure (gel transition). However, for the MCSH-I, the moduli dissipated slightly at 43 °C, then reached the plateau, possibly due to strong hydrophobic associations resulting in the dissociation of water molecules to the surface, as $(G', G'')_{MCSH\text{-}I} > (G', G'')_{MCH\text{-}I}$. Moreover, these interactions, i.e., increased salt strength, have also provided a negative shift to the gelation point by ≈10°C.

To demonstrate the flow characteristics of the hydrogels, the effect of shear rate on the viscosity was studied from 0.001 to 1000 s^{-1} (Figure S5, Supporting Information). It can be observed that both the samples exhibit a similarly pronounced shear thinning behavior, i.e., an increase in shear stress resulting in steep viscosity shrinkage, which could be attributed to the distortion of the hydrogel matrix by the shear stress due to disentanglement of the polymer network. This self-healing behavior after shear removal could aid in feasible large-scale smart window manufacturing, 3D printing of hydrogels for energy storage, and integration into the existing systems due to their ease of injection.[37]

The cellulose-based hydrogels are formed by the physical cross-linking of the polymer with the hydroxyl group (—OH) via hydrogen bonding (Figure 2D; Note S4, Supporting Information). Figure 2E demonstrates the binding of MC with the cations and anions dissociated from salts in the MCSH-I hydrogels. In addition to the physical cross-linking, dispersed salts demonstrate electrostatic, inter, and intra-molecular interactions: the sodium ions form coordinating bonding by competing with

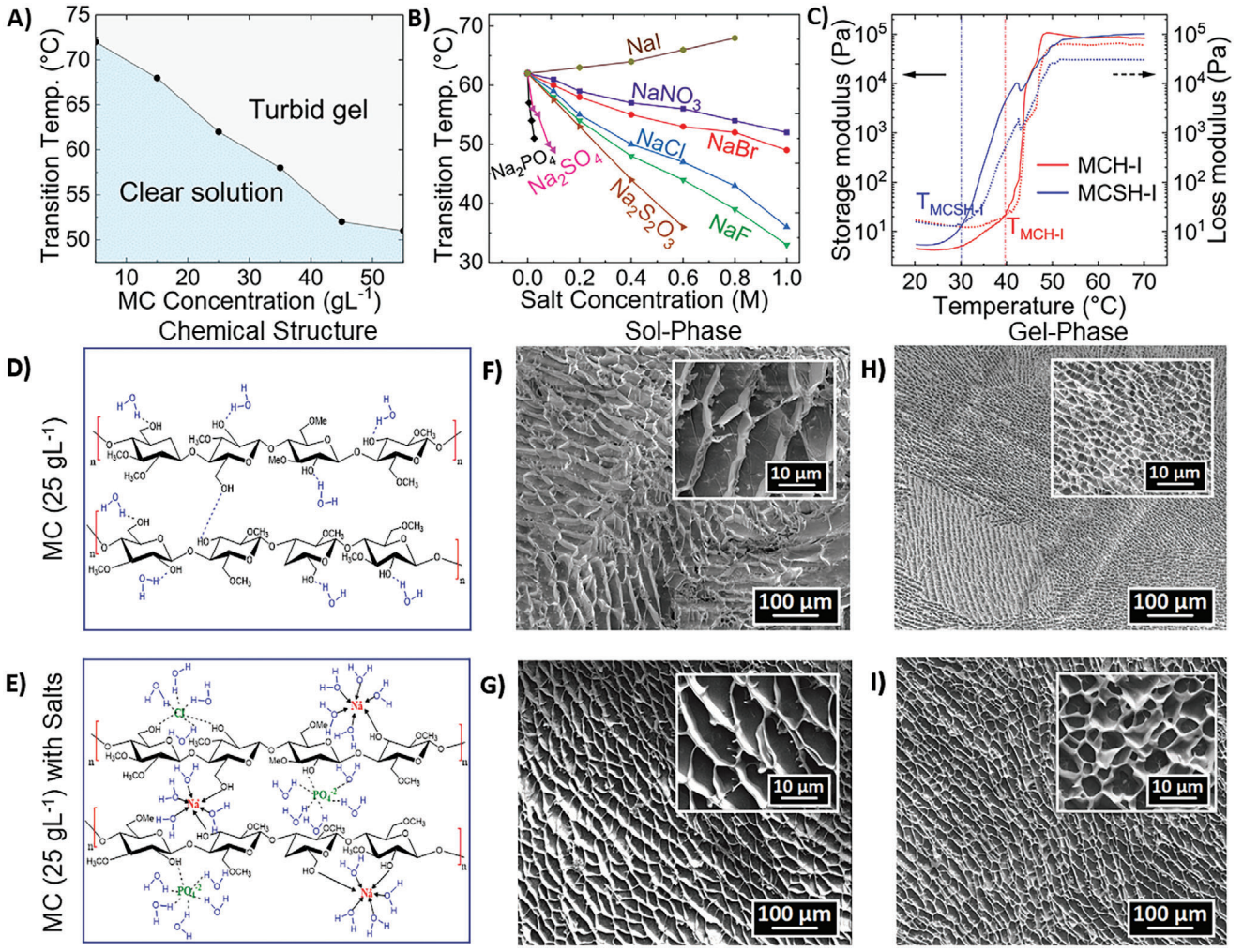

Figure 2. Transition temperature modulation and structural characterization of TR materials. A) Effect of cellulose concentration on the gelation temperature (temp.). B) LCST modulation as a function of single salt concentration. C) Rheological studies of MCH-I and MCSH-I samples at different temperatures. D,E) Structural linkages between methyl cellulose chains, water molecules, and salts in (D) MCH-I and (E) MCSH-I hydrogels. F–I) SEM images of TR materials before (F,H) and after phase change (G,I).

protons for the methoxy groups, while the anions exploit hydrogen bonding with the gelator molecule (Figure S6, Supporting Information).[38] The cationic dissolution connects the other sodium-linked-cellulose fibers through cooperative bonding, forming highly porous structures (Figure S7, Supporting Information). Cryo-SEM was utilized to analyze the interior morphological structures of MCH-I and MCSH-I before and after phase change (Figure 2F–I; Note S5, Supporting Information). Before phase change, the scaffold of both samples indicated a well-defined, interconnected, 3D porous honeycomb network that significantly facilitates the absorption of water molecules, enhancing thermo-sensitive characteristics. It is observed that the temperature has a trivial effect on the porosity (%) of the MCSH-I hydrogel (Figure S8, Supporting Information). On the contrary, the porosity (%) of the cellulose-based sample (MCH-I) reduced from 82% to 66%. The mean wall diameter of the MCH-I sample subsided from 2.2 nm (before phase change) to 0.7 nm (after phase change), while the percentage reduction was ≈30% for MCSH-I (Figure S9, Supporting Information). Conclusively, the cellulose polymer forms thermally stable interpenetrated structures as the temperature increases. The addition of salts (anions) has further activated this interlinkage, regulating the passage of incident solar radiation via light scattering. The formation of smaller pores results in sub-cooling and prolonged phase transition periods.[39,40] Since similar continuous interlinkages are formed in a 3D lattice, the solution becomes a "turbid gel."

2.2. Optical and Thermal Characterization of Thermos-Responsive Windows

For widespread applicability in real-time applications, smart windows should demonstrate dynamic solar transmittance while maintaining glass-like optical properties at room temperature. The MC window works on temperature-dependent tunable transmittance, i.e., solar transmittance when the temperature is below LCST, while demonstrating solar blockage as the

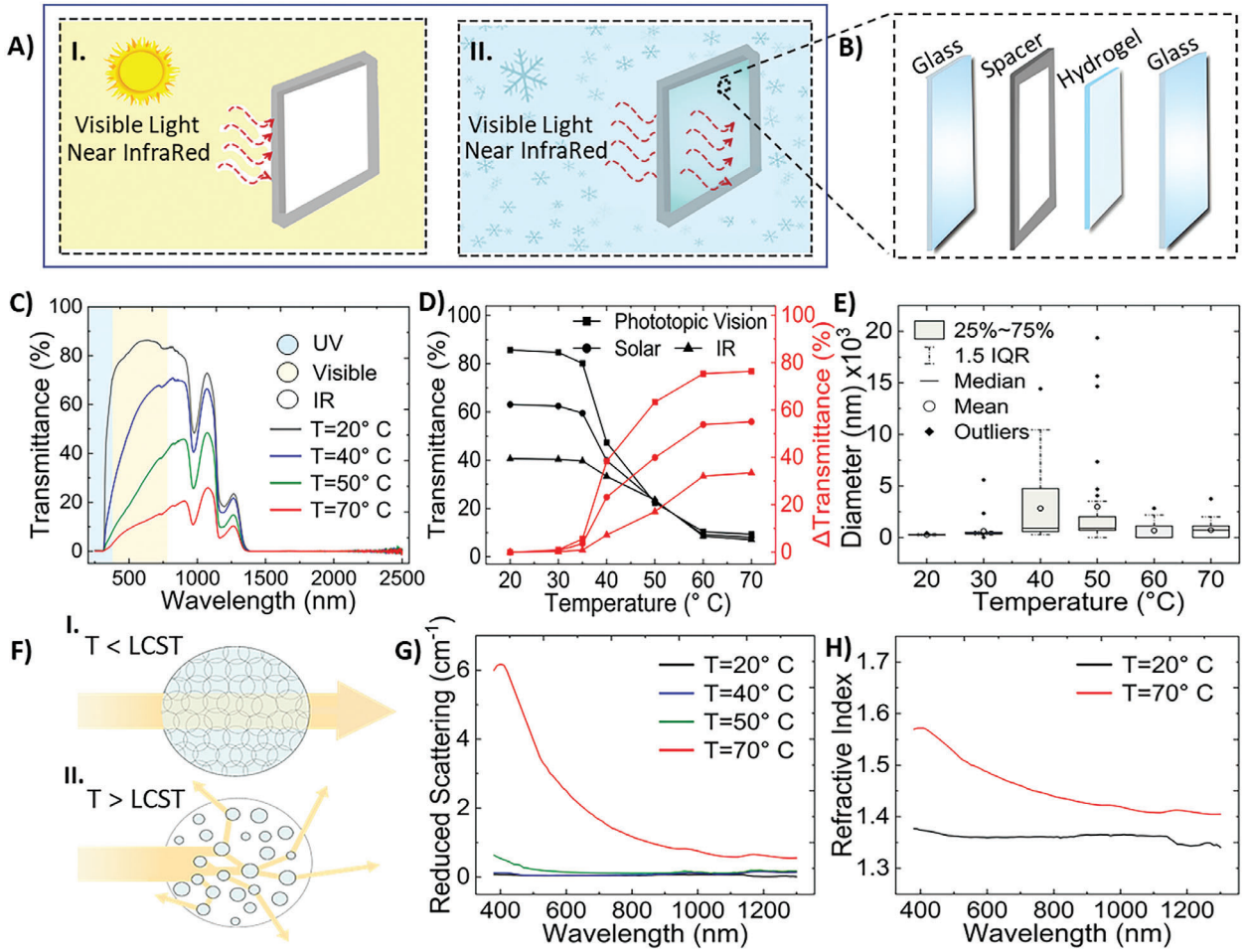

Figure 3. Optical and thermal characterization of thermo-responsive windows. A) Schematic representation of thermo-responsive window response during (A_I) summer and (A_{II}) winter conditions. B) Scheme of MCSH-I window panel. C) Transmittance spectra of MCSH-I hydrogels at different temperatures (T). D) Luminous, Solar, and IR transmittance (T_{Lum}, T_{solar}, and T_{IR}) and corresponding transmittance modulation (ΔT_{Lum}, ΔT_{solar}, and ΔT_{IR}) of MCSH-I window in response to temperature. E) Hydrodynamic diameters of MCSH-I hydrogel at different temperatures. Each analysis included a sample size (n) of 30 recordings. The grey box, (at 40 °C) represents the translucent or the onset of the transition, while the white box (at 70 °C) indicates opaque behavior. Whisker limits extend to ±1.5 times the Interquartile Range (IQR), which covers the middle 50% of the data (from 25% to 75%). Observations outside these limits were identified as outliers. F) Schematic representation of temperature-dependent scattering (F_I) before and (F_{II}) after phase transition. G) Reduced scattering coefficient of MCSH-I window at 20 °C, 40 °C, and 70 °C. H) The refractive index of the MCSH-I hydrogel at 20 °C and 70 °C.

temperature reaches the transition temperature (**Figure 3A**). In contrast to the more complex fabrication method, we employed a facile procedure to demonstrate the adaptability of this system to the existing windows. Hydrogel injection was achieved by allowing the hydrogel to flow freely into the spacer through gravity via a 1 cm diameter hole facilitated by a funnel (Figure 3B). Moreover, for large-scale production, alternative feasible methods, as described in Note S6 and Figure S10 (Supporting Information), can also be explored. A preliminary cost-benefit analysis indicates that manufacturing these systems entails a 40% higher cost than double-pane windows but offers a 20% cost advantage over low-E glass windows (Table S2, Supporting Information). It is worth noting that long-term energy savings could balance these higher upfront costs.

The performance of the TR windows is dependent upon the hydrogel's thickness.[21] To study this effect, spectral responses of the MCH-I and MCSH-I hydrogels at varying thicknesses (0.5, 10, and 15 mm) were analyzed (Note S7 and Figures S11–S12, Supporting Information). Thickness has a negligible effect (<3%) on the optical and thermal properties at temperatures below the LCST, resulting from the homogenous dispersion of water molecules that lead to high solar and visible light transmittance. Conversely, thicker samples delivered effective solar modulation after the phase change, as the increased thickness enabled longer path length for scattering, leading to increased opacity. 10 mm spacer-thick windows were chosen for further studies. This intelligently adaptive modulation leads to effective HVAC energy savings during peak load.[23,41]

The spectral response of MCSH-I before the phase change at 20 °C indicated a remarkably high intrinsic (≈89.3% over the entire spectrum) and optical (≈86.3% at 550 nm) transmittance, with relatively higher T_{solar} and IR transmittance (T_{IR})of 63% and

41%, respectively (Figure 3C; Figure S13, Supporting Information). After the phase change at ≈40 °C, T_{Lum}, T_{solar}, and T_{IR} significantly dropped to 47%, 40%, and 33%, respectively, signifying a robust thermal response of MC hydrogels (Figure 3D). Meanwhile, the solar reflectance (R_{solar}) increased from 7% (before the phase change) to 28% (after the phase change) (Figure S14, Supporting Information). As the temperature reaches 70 °C, the T_{Lum} of the MCSH-I window is modulated by ≈76% (from 86.3% to 10.3%), while the ΔT_{solar} is ≈55%, indicating strong thermal responsiveness and solar regulating capabilities. Notably, similar effects were recorded for the MCH-I material, showing the universality of the MC-based windows for different locations (Figures S15–S16, Supporting Information). Although the IR modulations are relatively modest (≈8%), these properties can be further optimized by employing methodologies such as altering polymer particle size, pitch length tuning, surface modification techniques, and incorporation of NIR-responsive materials.[28]

These results are considerably more efficient than its best available counterparts, such as VO_2 (TT ≈ 60 °C, ΔT_{solar} ≈ 9.3%), Liquid Crystals (ΔT_{solar} ≈ 16.45%), TET ($T_{Lum@20°C}$ ≈ 72%, ΔT_{solar} ≈ 51%), and hydroxypropyl cellulose-acrylamide (ΔT_{solar} ≈ 44%) windows.[25,28,42–44] Furthermore, the T_{Lum}, T_{solar}, and T_{IR} of the MCSH-I have not been affected (<3%) by consecutive 120 heating and cooling cycles, indicating TR repeatability, provided proper sealing to inhibit water evaporation (Figures S17–S18, Supporting Information). Durability tests conducted over 8 months of storage showed that these properties varied by <6%, demonstrating the resilience of these windows (Figure S19, Supporting Information). It is worth noting that the MC-hydrogels showed high stability and consistency without requiring the immersion of the de-swelled hydrogel in a solution of conductive polymer monomers, as in the case of PNIPAM hydrogels.[24]

The exhibited temperature-responsive phase transition is mainly due to the reversible hydrodynamic diametric swelling (Figure 3E). The hydrodynamic diameter of the MC-hydrogels at different temperatures was characterized by a DynaPro plate reader (Note S8, Supporting Information). The diameter of the MCSH-I below the LCST is about 300–600 nm and increases exponentially with temperature. After the transition point, at 40 °C and 50 °C, the formation of cellulosic hydrophobic associations (sol–gel transition) led to the swelling to ≈2800 and 6300 nm, respectively. However, at temperatures above 55 °C, these diameters drop significantly by 50% for every 10 °C rise due to the formation of 3D interlinkages throughout the hydrogel's matrix. This property of temperature-dependent hydrodynamic diameters results in effective refractive index and scattering modulations.[45–47]

To quantify the hydrogel's temperature-dependent absorption coefficient (μ_a) and reduced scattering coefficients (μ_s'), Monte Carlo simulations were used to fit these parameters based on the experimental spectral response of the MCSH-I thermos-responsive window (Figure S20, Supporting Information). Results show that, after phase change, the MC windows diffusely reflect the majority of the transmitted sunlight, while the solar weighted absorption coefficient in the visible range increased from $\mu_{a,\,20°C}$ ≈ 0.23 cm^{-1} to $\mu_{a,\,70°C}$ ≈ 0.48 cm^{-1} (Figure 3F; Figure S21, Supporting Information). Also, the reduced scattering increased significantly with temperature, particularly in the shorter wavelength visible light region with a peak at 400 nm, from μ_s' ≈ 0.046 cm^{-1} at 20 °C to 2.22 cm^{-1} at 70 °C (Figure 3G). This increase in reduced scattering coefficient is attributed to the phase change of the hydrogel, leading to a shift in scattering to longer wavelengths due to a rise in average scattering pore size.

From the reduced scattering coefficient, the effective refractive index of the matrix was further determined using the Mie and effective medium theory by assuming that the mixture of water and MC is the matrix, and the water pores are the spherical scatterers. The refractive index of the water-MC mixture was calculated by volume averaging the effective refractive index of the cellulose and water (Note S8–S9, Supporting Information). Results show a significant increase in the MC refractive index at 400 nm, from 1.37 at 20 °C to 1.57 at 70 °C (Figure 3H). The results indicate that the decreased size of the water pores and the increased refractive index of the matrix are needed to explain the enhanced scattering at high temperatures. Caution should be taken as the overall structure and the shapes that the matrix forms should play an important role, and those effects may have been lumped into the derived refractive index. Also, it can be noted that Beer–Lambert's law is not suitable for estimating scattering coefficients (Note S9, Supporting Information). This property of effective scattering and change in the refractive index makes MC windows promising for energy savings and other optoelectronic applications, such as tunable plasmonic hydrogel-based meta systems, beam steering, functional display materials, next-gen solar cells, and photocatalysis.[14,48]

2.3. Outdoor Demonstration and Performance of MC Smart Window

The prime factor in designing smart windows is to deliver substantial energy and environmental savings required for space cooling. To demonstrate these savings, we constructed a model with MCSH-I and a double pane window (20 cm × 20 cm × 1.2 cm) enclosed on the top of an insulated box (45 cm × 35 cm × 27 cm) (**Figure 4A$_I$**; Note S10, Supporting Information). A control lab experiment was conducted with a 500 W IR lamp as an irradiance source to illustrate the heat shielding capabilities (Figure 4A$_{II}$). The temperature of the double pane window rapidly increased from 20 °C to 85 °C after ≈30 min of illumination, signaling 65 °C increments with a heating rate of 2.17 °C min^{-1} (Figure 4B). In contrast, the MCSH-I window switched to a completely opaque state (gel-phase) after 16 min and had a significantly lower heating rate of 0.75°C min^{-1}, displaying only a 4.6 °C rise after the transition. When the lamp was turned OFF, the temperature of the double-pane window reduced beeline, reaching 44.5 °C in 30 mins, whereas the TR window temperature was reduced by only 8 °C. This rapid decrease in temperature of the double-pane window indicates sub-standard thermal shielding, while the gradual decline exhibited by MC-based TR windows manifests good thermal insulation.

The Overall Heat Transfer (U-factor), Solar Heat Gain Coefficient (SHGC), and Visible Transmittance are essential ratings to evaluate the performance ratings of the fenestration systems.[49] These ratings for the MCSH-I window were estimated using Window 7.8 (Figure 4C; Table S3, Supporting Information). Before the phase change, the MCSH-I window demonstrated a

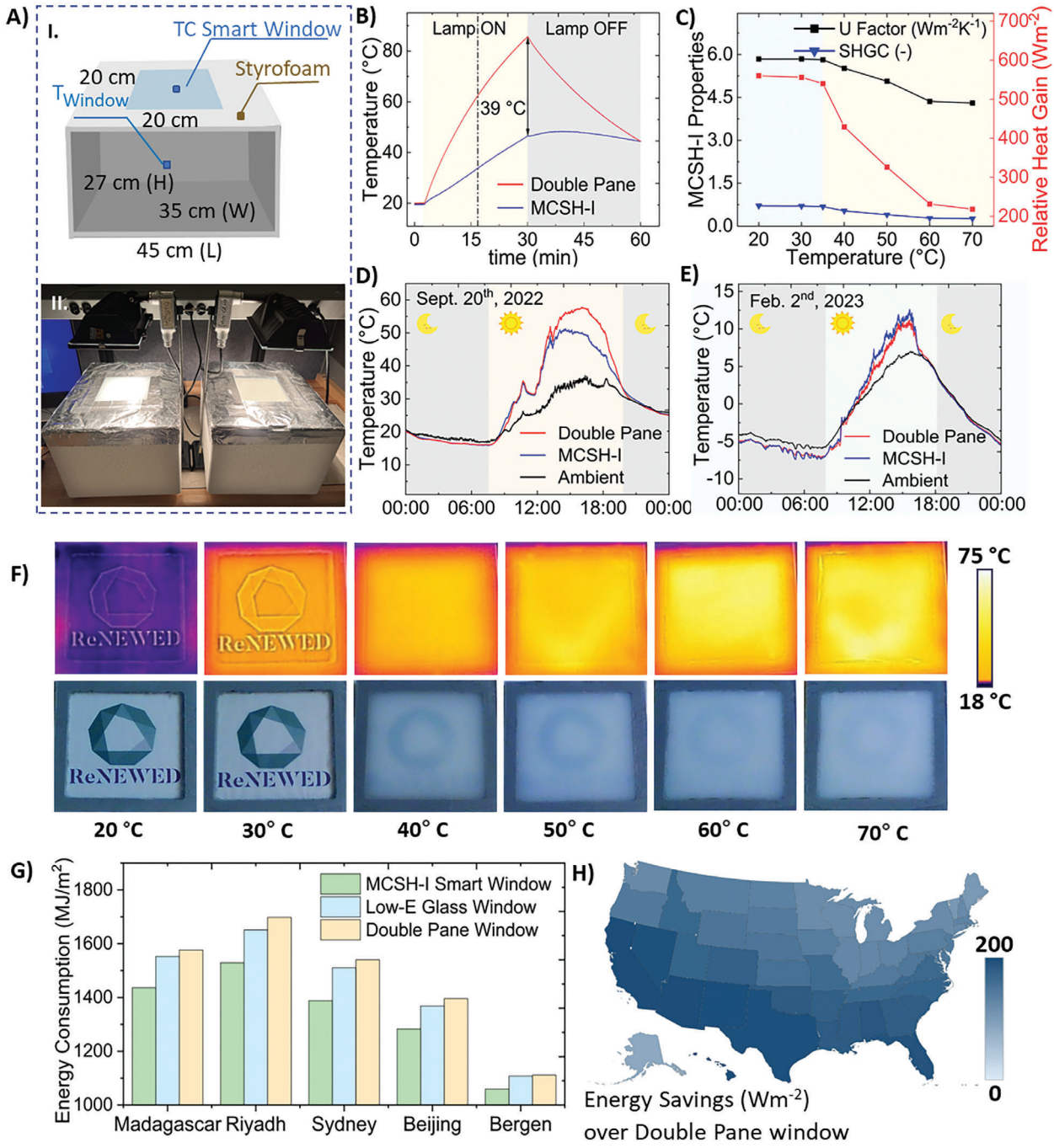

Figure 4. Performance characteristics of MCSH-I TR window. A)-(A_I) Schematics of outdoor demonstration setup for performance analysis. (A_{II}) In-lab demonstration of the heat shielding performance test. B) Heat shielding performance analysis under a solar lamp with dotted line indicating the moment of complete phase change. C) Estimated temperature-dependent performance metrics of MCSH-I windows. D,E) Temperature profiles of the proposed smart window surface compared with the Double pane window on a (D) mild sunny day and (E) winter day. The curves of the control test and the field test are smoothed using the simple moving average. F) Thermographic images of MCSH-I window from 20°C to 70°C. G) Simulated energy savings of MCSH-I window over the low-E and double pane window. H) Estimated energy savings of MCSH-I window against the double pane windows over the US.

relative heat gain of ≈500 W m^{-2} with a U-factor of 5.84 W m^{-2} K^{-1}. As the temperature increases, the relative heat gain is gradually reduced to 218 W m^{-2} (≈61% reduction) at 70 °C, while the U-factor decreases by 20%, indicating that MC hydrogels have excellent heat shielding capabilities, and their employment reduces the HVAC loads.

To exemplify the performance of the MC windows during summer and winter for real-time applications, the setup was placed on a rooftop of Herrick Labs in West Lafayette, Indiana

(Note S10, Supporting Information). The climate data: solar irradiation, relative humidity, and windspeed of both climates, summer (September 20, 2023) and winter (February 2, 2023), are documented (Figures S22–S23, Supporting Information). The temperature on the inner surface was recorded for comparison. During a hot day, the double pane window demonstrated the highest surface temperature of ≈54 °C, whereas the MCSH-I window displayed a relatively lower temperature of ≈46 °C during the daytime (Figure 4D). The inner surface (glass) temperature of the MCSH-I window was lower than the double pane window during peak load times between 11:00 AM and 4:30 PM, indicating that the room temperature is much lower, and a curtailed electrical load would be required for room cooling. On a cold day (−6 °C < T <7 °C), the smart window outperformed the double-pane window in solar absorbance and heat shielding, with a temperature difference of ≈5 °C above the double-pane window temperature (Figure 4E). This was due to high solar absorption in the IR region at temperatures below LCST. However, at night, temperatures of the MCSH-I glass window showed a minor difference of <3 °C, with surfaces being consistent with the ambient. The thermographic images at different temperatures were recorded using an IR camera (Figure 4F). As the temperature reaches above 40°C, the image on the other side of the window is barely visible, along with homogenous temperature distribution, indicating the potential of the MC windows for improved energy savings and controlled light transmission.

Energy simulations were conducted to evaluate the energy conservation that MCSH-I-based fenestration systems could achieve to a 91 m × 61 m × 3.35 m 12-story mid-rise office building (Figure S24, Supporting Information). Five major cities around the globe: Madagascar (Tropical), Riyadh (Arid), Sydney (Temperate), Beijing (Continental), and Bergen (Polar), were selected to represent the significant Koppen-Geiger climatic conditions.[50] Simulations show that MC-based TR windows would have positive energy savings in all climate zones (Table S3, Supporting Information). These savings are particularly significant when employed in dry, humid climatic zones (Tropical, Arid, and Temperate), with average annual savings of 154 MJ m^{-2} and 120 MJ m^{-2} over the extensively applied fenestration systems such as double plane and low-E glass windows (Figure 4G). Similarly, in polar climates, considerable savings of 50 MJ m^{-2} (on average) could be achieved by applying these TR systems. Moreover, studies were conducted to assess the potential savings of MC windows across the US (Figure 4H). Results suggest that using these windows leads to significant electric and economic savings, ranging from 5.49% to 11% and 4.34% to 8.56% compared to double-pane and low-E windows, respectively (Note S11, Supporting Information). Overall, the savings are notably higher over the southwest regions, with the largest being New Mexico, followed by Arizona, California, and Nevada, indicating their strong affinity to temperate climatic conditions (Figure S25, Supporting Information). These savings would translate to ≈0.014 metric tons of CO_2 eq. m^{-2} (AVERT 2020) (Note S12, Supporting Information). Although these savings may seem modest at the individual level, considering the large-scale deployment and ubiquity, these systems would lead to substantial carbon reductions and establish the promise of MCSH-I windows toward carbon neutrality and economic savings.

3. Conclusion

This work reports viable MC-based thermo-responsive materials with high cyclability and temperature-dependent optical performance tunability for energy-efficient windows and light management systems. The dynamic optical performance is triggered by the hydrophobic association between the methylcellulose and the water molecules (sol-gel transition), which can be effectively tuned from 34 °C to 72 °C by optimizing the MC and salt concentrations. The MC-based TR windows were fabricated by a simple approach and demonstrated superior optical transmittance at room temperature ($T_{Lum,\ double\text{-}pane\ glass}$ ≈ 82%, $T_{Lum,\ MCSH\text{-}I}$ ≈ 86%, and $T_{Lum,\ MCH\text{-}I}$ ≈ 85%) with enhanced solar modulation capabilities, ΔT_{Lum} ≈ 76%, ΔT_{solar} ≈ 53%, and ΔT_{IR} ≈ 33%. These reported properties are unprecedentedly higher than the proclaimed conventional VO_2 materials and other cellulose-based TR windows. Control experiments revealed that MC windows effectively provide heat shielding and mitigate the indoor room temperature by 39 °C with a twofold lower heating rate than the double pane window. Outdoor studies and simulations project an 8.2% and 6.4% reduction in HVAC loads (on average) compared to double-pane and low-E windows, respectively. At temperatures above the LCST, the windows exhibited tunable scattering (48× increase at 70 °C compared to 20 °C) and a change in refractive index, positioning them as prospective candidates for next-generation light management systems, including displays, photocatalysis, and thermo-optical switching. These savings are notably higher (11%) when implemented at temperature climatic zones. Featuring high stability, ease of scalability, and potential retrofitting capabilities to the current systems, our solution provides a practical and promising advancement for energy-efficient systems.

Supporting Information

Supporting Information is available from the Wiley Online Library or from the author.

Acknowledgements

The authors gratefully acknowledge the support from the David and Lucile Packard Foundation.

Conflict of Interest

The authors declare no conflict of interest.

Data Availability Statement

The data that support the findings of this study are available in the supplementary material of this article.

Keywords

building energy, energy saving, methylcellulose hydrogel, phase change material, smart window, thermochromic

Received: May 3, 2023
Revised: January 15, 2024
Published online:

[1] S. Courtney, U.S. Energy Information Administration—EA—ndependent Statistics and Analysis, https://www.eia.gov/todayinenergy/detail.php?id=47736 (February 2023).
[2] B. Fatih, The Future of Cooling—Analysis, https://www.iea.org/reports/the-future-of-cooling (February 2023).
[3] L. Pérez-Lombard, J. Ortiz, C. Pout, *Energy Build.* **2008**, *40*, 394.
[4] B. Nourozi, A. Ploskić, Y. Chen, J. Ning-Wei Chiu, Q. Wang, *Renewable Energy* **2020**, *162*, 2318.
[5] Y. Ke, J. Chen, G. Lin, S. Wang, Y. Zhou, J. Yin, P. S. Lee, Y. Long, *Adv. Energy Mater.* **2019**, *9*, 1902066.
[6] K. Menyhart, M. Krarti, *Build. Environ.* **2017**, *114*, 203.
[7] A. Shehabi, N. DeForest, A. McNeil, E. Masanet, J. Greenblatt, E. S. Lee, G. Masson, B. A. Helms, D. J. Milliron, *Energy Build.* **2013**, *66*, 415.
[8] R. Li, X. Ma, J. Li, J. Cao, H. Gao, T. Li, X. Zhang, L. Wang, Q. Zhang, G. Wang, C. Hou, Y. Li, T. Palacios, Y. Lin, H. Wang, X. Ling, *Nat. Commun.* **2021**, *12*, 1587.
[9] K.-W. Kim, T. Y. Yun, S.-H. You, X. Tang, J. Lee, Y. Seo, Y.-T. Kim, S. H. Kim, H. C. Moon, J. K. Kim, *NPG Asia Mater* **2020**, *12*, 84.
[10] M. Wang, X. Xing, I. F. Perepichka, Y. Shi, D. Zhou, P. Wu, H. Meng, *Adv. Energy Mater.* **2019**, *9*, 1900433.
[11] H. Kim, S. Yang, *Adv. Funct. Mater.* **2020**, *30*, 1902597.
[12] M.-H. Yeh, L. Lin, P.-K. Yang, Z. L. Wang, *ACS Nano* **2015**, *9*, 4757.
[13] D. Ruzmetov, S. D. Senanayake, S. Ramanathan, *Phys. Rev. B* **2007**, *75*, 195102.
[14] J. Lin, M. Lai, L. Dou, C. S. Kley, H. Chen, F. Peng, J. Sun, D. Lu, S. A. Hawks, C. Xie, F. Cui, A. P. Alivisatos, D. T. Limmer, P. Yang, *Nature Mater.* **2018**, *17*, 261.
[15] A. S. R. Bati, Y. L. Zhong, P. L. Burn, M. K. Nazeeruddin, P. E. Shaw, M. Batmunkh, *Commun. Mater.* **2023**, *4*, 2.
[16] M. Li, S. Magdassi, Y. Gao, Y. Long, *Small* **2017**, *13*, 1701147.
[17] D. Kolenatý, J. Vlček, T. Bárta, J. Rezek, J. Houška, S. Haviar, *Sci. Rep.* **2020**, *10*, 11107.
[18] J. Zhang, J. Li, P. Chen, F. Rehman, Y. Jiang, M. Cao, Y. Zhao, H. Jin, *Sci. Rep.* **2016**, *6*, 27898.
[19] Y. Cui, Y. Ke, C. Liu, Z. Chen, N. Wang, L. Zhang, Y. Zhou, S. Wang, Y. Gao, Y. Long, *Joule* **2018**, *2*, 1707.
[20] J. Li, P. Gu, H. Pan, Z. Qiao, J. Wang, Y. Cao, W. Wang, Y. Yang, *Adv. Sci.* **2023**, *10*, 2206044.
[21] Y. Zhou, S. Wang, J. Peng, Y. Tan, C. Li, F. Y. C. Boey, Y. Long, *Joule* **2020**, *4*, 2458.
[22] H. Y. Lee, Y. Cai, S. Bi, Y. N. Liang, Y. Song, X. M. Hu, *ACS Appl. Mater. Interfaces* **2017**, *9*, 6054.
[23] X.-H. Li, C. Liu, S.-P. Feng, N. X. Fang, *Joule* **2019**, *3*, 290.
[24] Y. Shi, C. Ma, L. Peng, G. Yu, *Adv. Funct. Mater.* **2015**, *25*, 1219.
[25] S. Wang, T. Jiang, Y. Meng, R. Yang, G. Tan, Y. Long, *Science* **2021**, *374*, 1501.
[26] D. Yu, S. Zhuo, J. Wang, Z. Liu, J. Ye, Y. Wang, L. Chen, X. Ouyang, K. Zhang, X. Zhou, J. Guan, Y. Liu, W. Chen, L. Liao, M. Zhuo, *Small* **2023**, *19*, 2205833.
[27] X. Zhao, W. Yao, J. Sun, J. Yu, J. Ma, T. Liu, Y. Lu, R. Hu, X. Jiang, *Chem. Eng. J.* **2023**, *460*, 141715.
[28] A. Nakamura, R. Ogai, K. Murakami, *Sol. Energy Mater. Sol. Cells* **2021**, *232*, 111348.
[29] T. Li, C. Chen, A. H. Brozena, J. Y. Zhu, L. Xu, C. Driemeier, J. Dai, O. J. Rojas, A. Isogai, L. Wågberg, L. Hu, *Nature* **2021**, *590*, 47.
[30] G. G. D. Han, H. Li, J. C. Grossman, *Nat. Commun.* **2017**, *8*, 1446.
[31] Y.-B. Lei, H.-X. Xia, K. Chen, A. Plenković-Moraj, W. Huang, G. Sun, *Plant Sci.* **2021**, *311*, 111020.
[32] J. Zhang, Q. Li, C. Dai, M. Cheng, X. Hu, H. Kim, H. Yang, D. J. Preston, Z. Li, X. Zhang, W. Lee, *Small* **2022**, *18*, 2205057.
[33] L. Li, P. M. Thangamathesvaran, C. Y. Yue, K. C. Tam, X. Hu, Y. C. Lam, *Langmuir* **2001**, *17*, 8062.
[34] Y. Xu, L. Li, P. Zheng, Y. C. Lam, X. Hu, *Langmuir* **2004**, *20*, 6134.
[35] P. Xavier, P. Rao, S. Bose, *Phys. Chem. Chem. Phys.* **2016**, *18*, 47.
[36] Y. Xu, C. Wang, K. C. Tam, L. Li, *Langmuir* **2004**, *20*, 646.
[37] M. Caprioli, I. Roppolo, A. Chiappone, L. Larush, C. F. Pirri, S. Magdassi, *Nat. Commun.* **2021**, *12*, 2462.
[38] R. R. A. Silva, P. A. V. de Freitas, S. C. Teixeira, T. V. de Oliveira, C. S. Marques, P. C. Stringheta, A. C. dos Santos Pires, S. O. Ferreira, N. de Fátima Ferreira Soares, *Food Biophys.* **2022**, *17*, 59.
[39] S. S. Sundarram, W. Li, *Appl. Therm. Eng.* **2014**, *64*, 147.
[40] Y. Yamagishi, T. Sugeno, T. Ishige, H. Takeuchi, A. T. Pyatenko, in *Proc. 31st Intersoc. Energy Conv. Eng. Conf.*, IEEE, Washington, DC, USA, **1996**, pp. 2077–2083.
[41] X. Shi, T. Abel, L. Wang, *Sol. Energy* **2020**, *201*, 561.
[42] Y.-S. Yang, Y. Zhou, F. B. Yin Chiang, Y. Long, *RSC Adv.* **2016**, *6*, 61449.
[43] W. Meng, Y. Gao, X. Hu, L. Tan, L. Li, G. Zhou, H. Yang, J. Wang, L. Jiang, *ACS Appl. Mater. Interfaces* **2022**, *14*, 28301.
[44] S. Wang, Y. Zhou, T. Jiang, R. Yang, G. Tan, Y. Long, *Nano Energy* **2021**, *89*, 106440.
[45] M. J. Rozin, D. A. Rosen, T. J. Dill, A. R. Tao, *Nat. Commun.* **2015**, *6*, 7325.
[46] Y. Zhai, Y. Ma, S. N. David, D. Zhao, R. Lou, G. Tan, R. Yang, X. Yin, *Science* **2017**, *355*, 1062.
[47] K. Yao, Q. Meng, V. Bulone, Q. Zhou, *Adv. Mater.* **2017**, *29*, 1701323.
[48] F. Neubrech, X. Duan, N. Liu, *Sci. Adv.* **2020**, *6*, eabc2709.
[49] I. National Fenestration Rating Council, **2013**.
[50] H. E. Beck, N. E. Zimmermann, T. R. McVicar, N. Vergopolan, A. Berg, E. F. Wood, *Sci. Data* **2018**, *5*, 180214.